Rod Photopigment Kinetics After Photodisruption of the Retinal Pigment Epithelium

Benjamin D. Masella,[1,2] Jennifer J. Hunter,[2,3] and David R. Williams[1–3]

[1]The Institute of Optics, University of Rochester, Rochester, New York, United States
[2]Center for Visual Science, University of Rochester, Rochester, New York, United States
[3]Flaum Eye Institute, University of Rochester, Rochester, New York, United States

Correspondence: Benjamin D. Masella, 55 Black Brook Road, Keene, NH 03431, USA; bmasella@cvs.rochester.edu.

Submitted: December 18, 2013
Accepted: July 18, 2014

Citation: Masella BD, Hunter JJ, Williams DR. Rod photopigment kinetics after photo-disruption of the retinal pigment epithelium. *Invest Ophthalmol Vis Sci*. 2014;55:7535–7544. DOI:10.1167/iovs.13-13796

Purpose. Advances in retinal imaging have led to the discovery of long-lasting retinal changes caused by light exposures below published safety limits, including disruption of the RPE. To investigate the functional consequences of RPE disruption, we combined adaptive optics ophthalmoscopy with retinal densitometry.

Methods. A modified adaptive optics scanning light ophthalmoscope (AOSLO) measured the apparent density and regeneration rate of rhodopsin in two macaques before and after four different 568-nm retinal radiant exposures (RREs; 400–3200 J/cm^2). Optical coherence tomography (OCT) was used to measure the optical path length through the photoreceptor outer segments before and after RPE disruption.

Results. All tested RREs caused visible RPE disruption. Apparent rhodopsin density was significantly reduced following 1600 ($P = 0.01$) and 3200 J/cm^2 ($P = 0.007$) exposures. No significant change in apparent density was observed in response to 800 J/cm^2. Surprisingly, exposure to 400 J/cm^2 showed a significant increase in apparent density ($P = 0.047$). Rhodopsin recovery rate was not significantly affected by these RREs. Optical coherence tomography measurements showed a significant decrease in the optical path length through the photoreceptor outer segments for RREs above 800 J/cm^2 ($P < 0.001$).

Conclusions. At higher RREs, optical path length through the outer segments was reduced. However, the rate of photopigment regeneration was unchanged. While some ambiguity remains as to the correlation between measured reflectivity and absolute rhodopsin density; at the lowest RREs, RPE disruption appears not to be accompanied by a loss of apparent rhodopsin density, which would have been indicative of functional loss.

Keywords: light damage, retinal pigment epithelium, rhodopsin regeneration, densitometry, dark adaptation

A complete description of the consequences of light exposure for the retina demands a functional as well as a structural assessment. Due to the absorptive pigments it contains, the photoreceptor/RPE complex in the outer retina is especially susceptible to phototoxic effects,[1] suggesting that the most informative functional measures would specifically target these layers. A critically important role of this complex is the isomerization and regeneration of the visual pigment. Retinal densitometry provides an objective way to estimate photopigment optical density and kinetics.[2–10] Masella et al.[11] recently described a retinal densitometer integrated into an adaptive optics scanning light ophthalmoscope (AOSLO) that is capable of resolving single cells in the living primate eye.

As an initial application of adaptive optics (AO) retinal densitometry, we have chosen to investigate an unexpected phototoxic phenomenon for which the functional consequences are currently unknown. By imaging RPE cell autofluorescence in vivo with an AOSLO, Morgan et al.[12] found that a retinal radiant exposure as low as 247 J/cm^2 at 568 nm, which lay below the maximum permissible exposure at the time, caused a disruption in the otherwise regular pattern of lipofuscin fluorescence. This RPE disruption is photochemical in nature, occurs less than 1 week after exposure, and appears to be permanent.[12] Here, we used AO retinal densitometry to determine whether exposure to bright visible light resulting in RPE disruption compromises the visual cycle in small patches of retina (on the order of 0.01 mm^2).

Methods

Animal Preparation

The experiments in this study were performed using macaque monkeys and were approved by The University of Rochester's Committee on Animal Resources (Rochester, NY, USA) and the study complied with the ARVO Statement for the Use of Animals in Ophthalmic and Vision Research. We have previously published details about the experimental preparation and the two primates used in this investigation.[11] Before each imaging experiment, the animal was injected with ketamine (18–21.5 mg/kg), glycopyrrolate (0.017 mg/kg), ketofen (5 mg/kg) and, when available, valium (0.25 mg/kg). During imaging, the animal was intubated and anesthetized with isoflurane gas. To prevent large eye movements, the animal was paralyzed with vecuronium bromide (60 μg/kg/h). Pupils were dilated and the eye cyclopleged with 1 to 2 drops

each of phenylephrine hydrochloride (2.5%) and tropicamide (1%). A lid speculum was used to hold the imaged eye open and a hard contact lens protected the cornea and corrected some refractive error. A head post, gimbal mount, and three-axis stage were used to align the animal's head and pupil with the AOSLO and allow for stable control of retinal image location.

Apparatus

Imaging of the RPE, densitometry measurements, and RREs were all performed with an AOSLO that has been previously described.[11,13] It is a point-scanning system that scans the retina in a raster pattern with a 25-Hz frame rate. An infrared laser diode (850 nm) was used in conjunction with a custom Shack-Hartmann wavefront sensor to measure the monochromatic aberrations of the eye. These aberrations were then corrected using a deformable mirror (ALPAO DM97-15; ALPAO, Biviers, France). The AOSLO was used to simultaneously collect images with infrared (superluminescent diode, 790 nm Δ17 nm) and visible (Argon/Krypton laser, 514 nm or 568 nm) wavelengths. Photomultiplier tubes (Hamamatsu H7422-40/-50; Hamamatsu, Hamamatsu, Japan) were used for detection. An acousto-optic modulator (AOM) and a mechanical shutter were used in conjunction with the Argon/Krypton (ArKr) laser for precise control of visible light exposures. To image the RPE, the fluorescence of lipofuscin was excited using 568 nm and imaged with an emission filter centered at 624 nm (Δ40 nm).[14]

AO Retinal Densitometry

The time course of rhodopsin recovery was tracked by first dark-adapting the entire retina for 1 hour, then using the 514-nm laser to record 2° × 2° images with the 514-nm source at a low scotopic energy density (1.7×10^5 scot Td·s) before and after a 514-nm bleach in the central ⅓° × ½° retinal area (2-second bleach ranging from 3.6×10^7 scot Td·s to 8.4×10^7 scot Td·s). Videos were recorded at 2.5, 5, 7.5, 10, 15, 20, 25, 30, and 35 minutes after the bleach.

Data from the densitometry measurements were processed using the methods described in Masella et al.[11] The apparent density measurement made in this study is given by the following equation:

$$D_{apparent} = log_{10}\left[\frac{R_{in,b}}{R_{out,b}} / \frac{R_{in,d}}{R_{out,d}}\right] \quad (1)$$

where R_{in} and R_{out} represent the average reflectance measured inside and outside the bleached region of the image, respectively, and the subscripts b and d indicate measurements taken in the bleached and dark adapted states, respectively.

The time course of rhodopsin recovery was assumed to follow rate-limited kinetics as described by Mahroo and Lamb in 2004.[7] The average of the four recovery measurements taken in each retinal location was fit using this equation:

$$D(t) = D_{apparent} \cdot K_m \cdot W\left\{\left(\frac{B}{K_m}\right)e^{\left(\frac{B}{K_m}\right)}e^{-\left(\frac{1-K_m}{K_m}\right)vt}\right\} \quad (2)$$

where, $D(t)$ is the instantaneous apparent density at time t, $D_{apparent}$ is the effective dark-adapted rhodopsin density, B is the fraction of rhodopsin bleached, t is time from the bleach, W is the Lambert W function, and K_m is analogous to the Michaelis constant in enzyme kinetics.[15] As previously reported by Masella et al.,[11] the best-fit value of K_m in healthy retina was found to be 0.2, and this value was used throughout this study. The experimental data is used to fit the variables $D_{apparent}$ and v, which is the initial rate of rhodopsin recovery. When fitting the regeneration time course, the data point immediately following the bleach ($t = 0$) was excluded because the normalization region was partially bleached at that time, but was assumed to be fully dark adapted after 2.5 minutes. The extinction ratio of the AOM used to confine the bleaching exposure to the central area of interest was approximately 100:1. Thus, the area of the retina over which the AOM was in its off state would receive an exposure large enough to cause a 3% reduction of rhodopsin concentration in the retinal region intended for normalization of the density measurements. Initial rhodopsin recovery rates for human subjects have been previously reported to be approximately 9% per minute,[8] and Masella et al.[11] found recovery rates of the two animals in this study to be approximately 7% per minute. Thus, the surrounding region of the retina should have recovered to better than 99% of the dark-adapted state before the 2.5-minute measurement has occurred.

Procedure

To obtain an accurate baseline measure of rhodopsin kinetics prior to a potentially damaging 568-nm exposure, four initial bleach and recovery measurements were made in each location using the method described by Masella et al.[11] Due to the time-consuming nature of these measurements and a self-imposed limit of 6 hours of anesthesia time for each animal per week, these pre-exposure measurements were made on two separate days approximately 1-week apart.

Exposures designed to produce RPE disruption were delivered approximately 1 week after the second set of pre-exposure measurements in the same locations as the small area bleach. The wavelength of the radiant exposures was 568 nm. We used RREs of 400, 800, 1600, and 3200 J/cm^2. Table 1 shows the 568-nm power and duration for each radiant exposure level as well as its relation to the maximum permissible exposure (MPE) defined by the American National Standards Institute (ANSI Z136.1-2007). Each RRE was tested in four different locations centered close to the rod peak (~15° from the fovea), two locations in each of the two monkeys. To match previous studies of RPE disruption,[12,16] these RREs were delivered in ½° × ½° square retinal areas.

The 568-nm exposures were delivered through the AOSLO using methods similar to previous studies of RPE disruption.[1,12,16] During each exposure, the scan size of the AOSLO was reduced to a ½° raster. The source was set at its maximum intensity on that day and the exposure duration was adjusted to produce the desired RRE. The retina was continually monitored to insure that the exposure location remained constant.

Table 1. Experimental Parameters for All 568-nm Retinal Radiant Exposures Tested

RRE, J/cm^2	Power Incident on Cornea, μW	Exposure Duration, s	Fraction of ANSI Photochemical MPE
400	310	221	0.7
800	295	465	1.4
1600	333	823	2.9
3200	260	2109	5.7

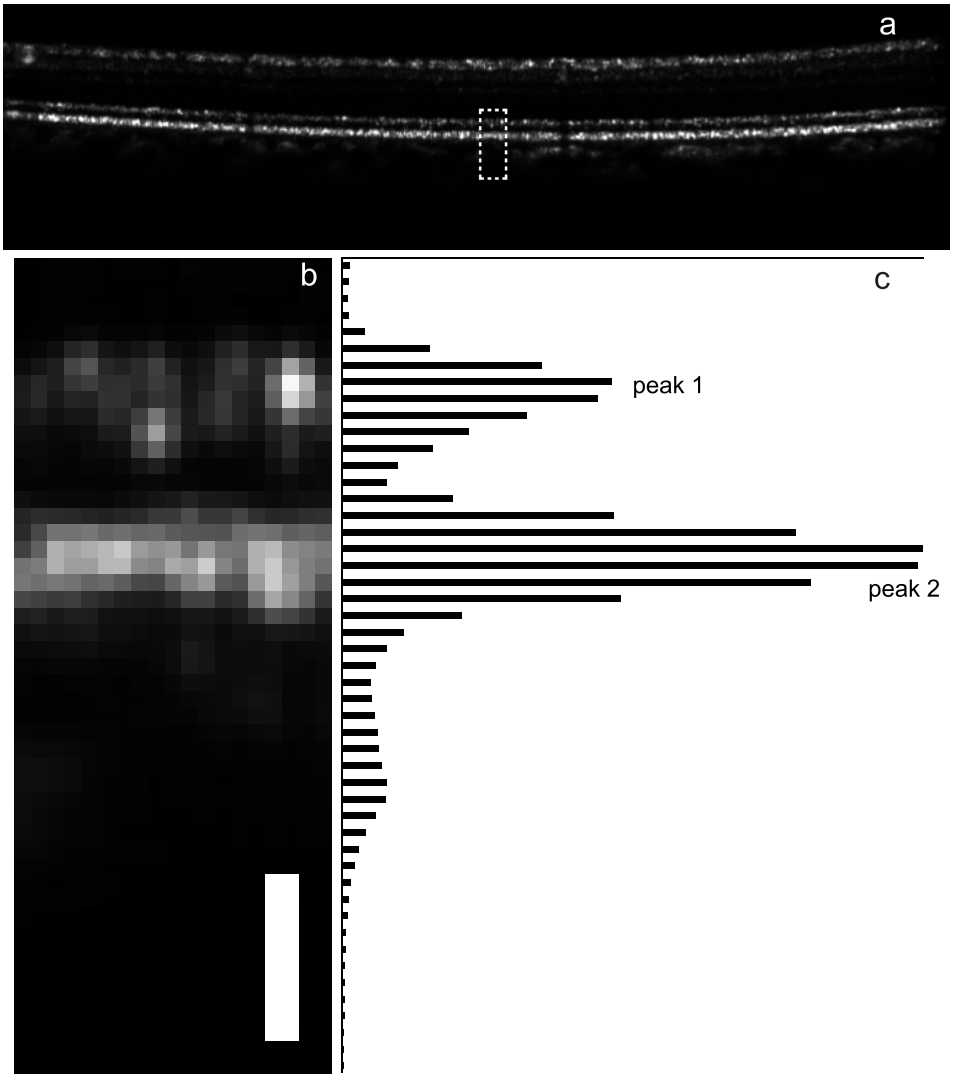

FIGURE 1. Representative OCT data used to test whether 568-nm exposures had an effect on the photoreceptors or RPE. (**A**) Linear data from a single B-Scan through the center of a tested region (pre-exposure). The *dashed rectangle* delineates the area of retina to be tested. (**B**) Expanded image of the retinal area of interest. (**C**) Mean signal intensity as a function of depth calculated from all B-Scans that passed through the retinal area of interest. Primary peaks used in subsequent depth analysis are labeled as peak 1 and peak 2.

Two weeks after the 568-nm exposures (a length of time that allowed for the onset of RPE disruption and any initial healing), two rhodopsin recovery measurements were made in each location. An additional two measurements were made the following week.

Optical Coherence Tomography (OCT)

Wide-field SLO and OCT images of the retina were obtained before and after each RRE using the Heidelberg Spectralis HRA+OCT (Heidelberg Engineering, Heidelberg, Germany). This instrument takes 30° field of view (FOV) images using four imaging modalities: IR reflectance (815 nm), red-free reflectance (488 nm), blue-light autofluorescence (AF; excitation 488 nm, emission above 510 nm), and infrared autofluorescence (IRAF; excitation 785 nm, emission 805–840 nm). It also uses Fourier-domain OCT to capture 3-dimensional volume data of the retina.

To interpret the volume of OCT data collected at each location, it was necessary to first identify the location of the ½° exposed region within the much larger area scanned by the HRA (approximately 16° × 6°). We used image processing software, ImageJ software (http://imagej.nih.gov/ij/; provided in the public domain by the National Institutes of Health, Bethesda, MD, USA), to parse each OCT volume scan and save it as a series of 32-bit TIFF images, each representing a single axial slice (B-scan). An 8-bit, en face projection was also generated from each OCT volume. Adobe Photoshop (Adobe Systems, Inc., San Jose, CA, USA) was then used to overlay and align the OCT projection onto a simultaneously acquired IR SLO image. Comparison of these overlaid images to images of the same retinal location in AF or IRAF mode and to AOSLO images allowed for manual identification of the transverse position of the exposed area within the OCT volume. Mathworks Matlab (Mathworks, Natick, MA, USA) was then used to reslice the OCT volume, pixel-by-pixel, into depth slices, each containing pixels associated with a single, axial retinal layer. Because each OCT scan was purposely centered on the retinal location of interest, curvature of the OCT image was not an issue (i.e., retinal layers were parallel to the horizontal B-scan pixels in the portion of the volume containing the retinal region of interest). Once the volume had been resliced, the mean intensity within the exposed region was calculated at each depth. Figure 1A

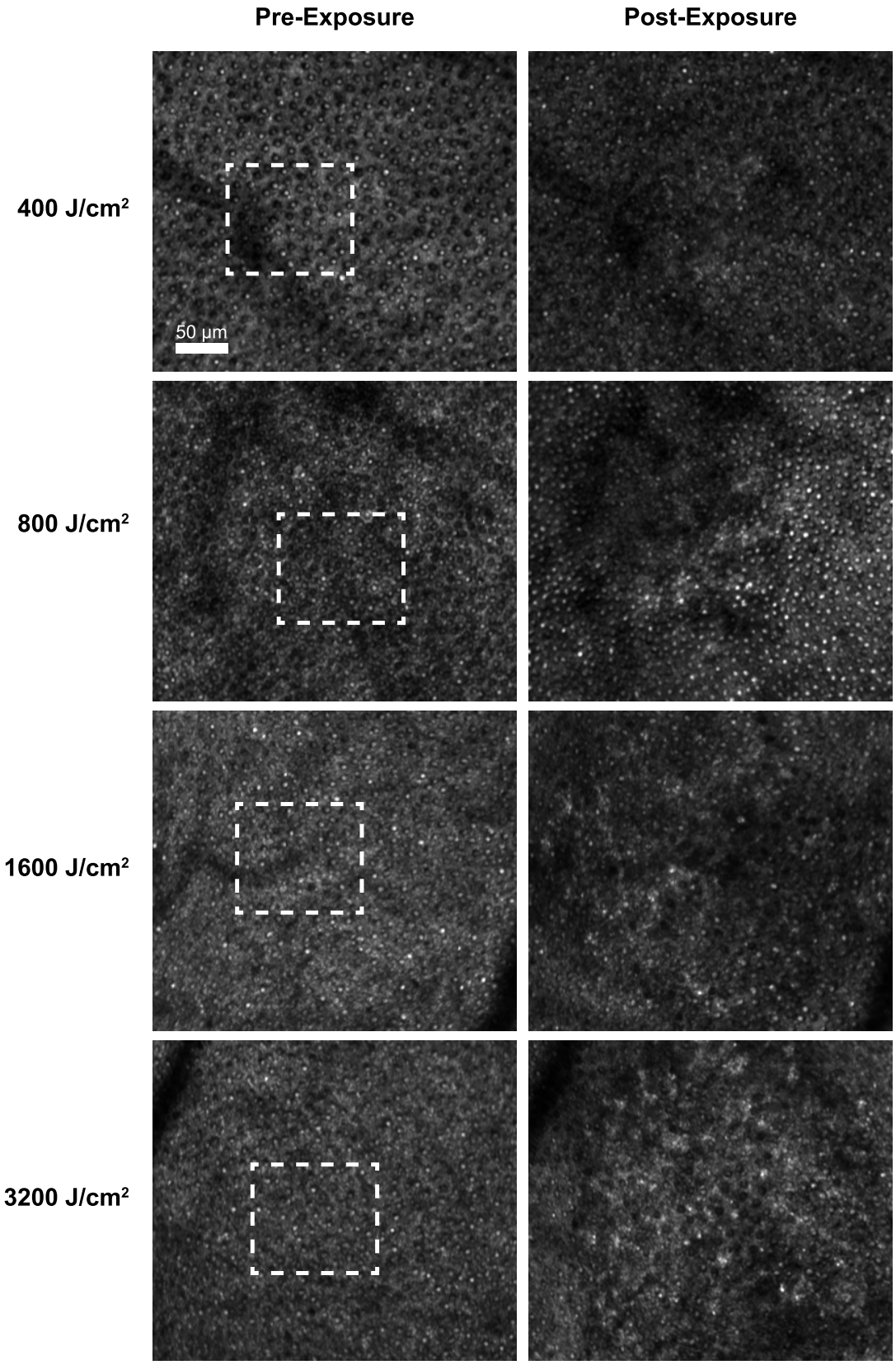

FIGURE 2. Representative in vivo IR reflectance images from the AOSLO taken before and after 568-nm radiant exposures. The *white boxes* indicate the exposure locations. Post exposure images at all exposure levels show changes in photoreceptor reflectance.

Investigative Ophthalmology & Visual Science

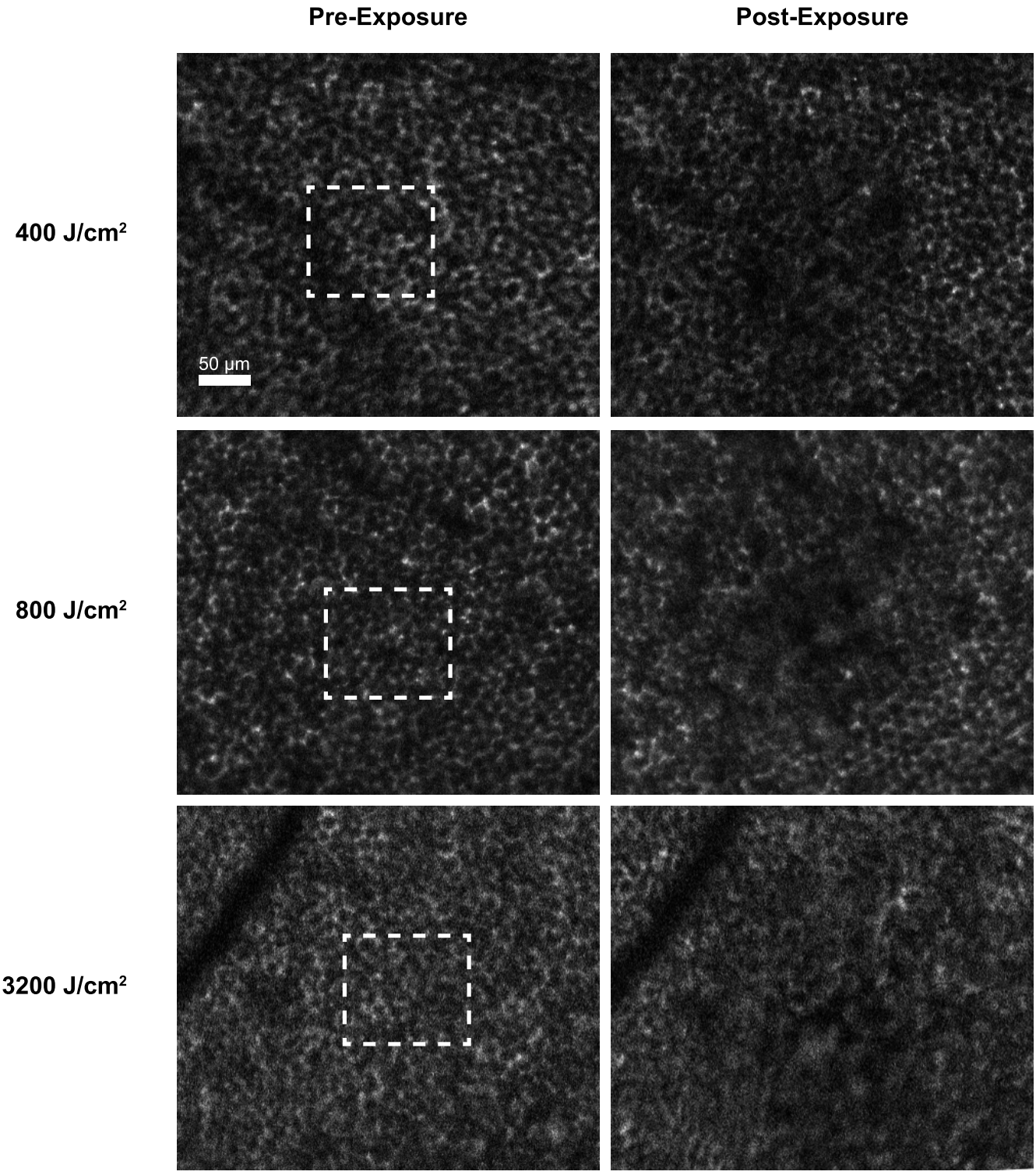

FIGURE 3. Representative in vivo RPE fluorescence images from the AOSLO taken before and after 568-nm radiant exposures. The *white boxes* indicate the exposure location. Retinal pigment epithelial disruption is visible at all retinal radiant exposures.

shows a representative OCT B-Scan of the retina that passes through an exposed region. Figures 1B and 1C show the portion of this B-Scan containing photoreceptor reflectance in a ½° test region and the average intensity as a function of depth calculated from all the B-Scans that passed through the exposed area, respectively. The relative peak positions of the two primary signal peaks in the outer retina associated with the photoreceptors and RPE were quantified by modeling each as a Gaussian distribution.

Statistical Analysis

ANOVAs were used to test for significant effects of RRE on apparent rhodopsin density, initial recovery rate and OCT

Table 2. Best Values for $D_{apparent}$ and v From Weighted, Least-Squares Fitting of Densitometry Measurements From Each Location Tested

		Pre-Exposure*		Post Exposure	
RRE, J/cm²	Animal	$D_{apparent}$	v, min⁻¹	$D_{apparent}$	v, min⁻¹
400	1	0.084	0.084	0.102	0.091
		0.075	0.074	0.095	0.085
	2	0.033	0.058	0.053	0.084
		0.023	0.070	0.036	0.052
800	1	0.100	0.066	0.018	0.076
		0.086	0.079	0.022	0.082
	2	0.022	0.082	0.029	0.082
		0.034	0.080	0.020	0.061
1600	1	0.045	0.041	0.040	0.069
		0.067	0.061	0.039	0.081
	2	0.047	0.080	0.030	0.054
		0.044	0.066	0.028	0.053
3200	1	0.064	0.048	0.034	0.051
		0.065	0.062	0.026	0.047
	2	0.028	0.062	0.010	0.043
		0.025	0.051	0.025	0.065

Each RRE was tested in two retinal locations in each animal.
* The pre-exposure values have been previously reported.[11]

optical path length measurements. In addition, the apparent density before and after 568-nm exposure were compared using a two-tailed student's *t*-test, assuming equal variance. Optical coherence tomography measurements before and after 568-nm exposure were also tested in this way. No correction for multiple comparisons was applied in any of the analyses. A *P* value less than 0.05 was deemed significant. All error ranges reported are the SEM.

Results

As expected, all of the RREs tested caused visible disruption of RPE autofluorescence. Changes in IR reflectance of the photoreceptor layer are also visible at each RRE. Figures 2 and 3 show representative photoreceptor reflectance and RPE fluorescence images before and after various exposures.

As previously reported,[11] the average apparent densities before 568-nm exposure were 0.073 ± 0.006 for animal 1 and 0.032 ± 0.003 for animal 2. Average initial recovery rates for these animals were 0.064 ± 0.005 min⁻¹ and 0.069 ± 0.004 min⁻¹, respectively.

The resulting apparent densities and initial recovery rates before and after each tested RRE are shown in Table 2. Figure 4 shows the apparent density time courses measured in a representative retinal location, before and after a 3200 J/cm² exposure in animal 1. While the mean initial recovery rate of rhodopsin after each RRE was slightly larger than the pre-exposure mean, statistical analysis showed that RRE had no significant effect on recovery rate (ANOVA, $P = 0.99$; student's

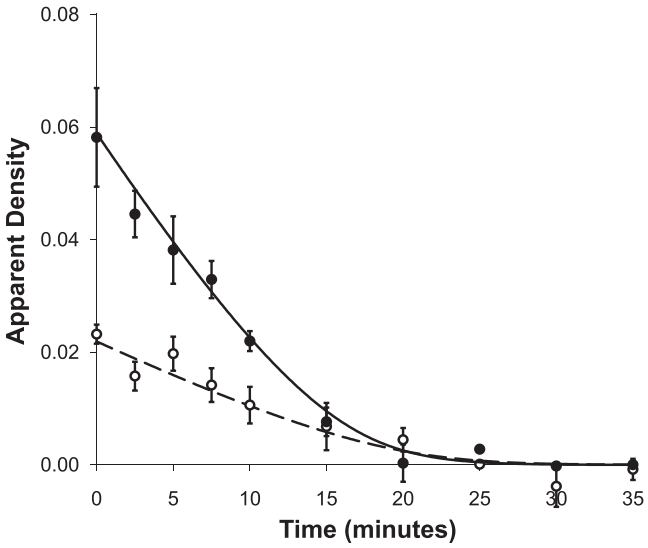

Figure 4. Apparent density time courses measured in a representative retinal location, before and after a 3200 J/cm² exposure in animal 1. *Closed circles* represent pre-exposure data and *open circles* represent post exposure data. The *solid line* is the rate-limited kinetics model with $B = 0.88$, $D_{apparent} = 0.053$, $v = 0.047$ min⁻¹, and $K_m = 0.2$. The *dashed line* is the same model with $B = 0.90$, $D_{apparent} = 0.024$, $v = 0.051$ min⁻¹, $K_m = 0.2$. The $t = 0$ time point was excluded from both fits.

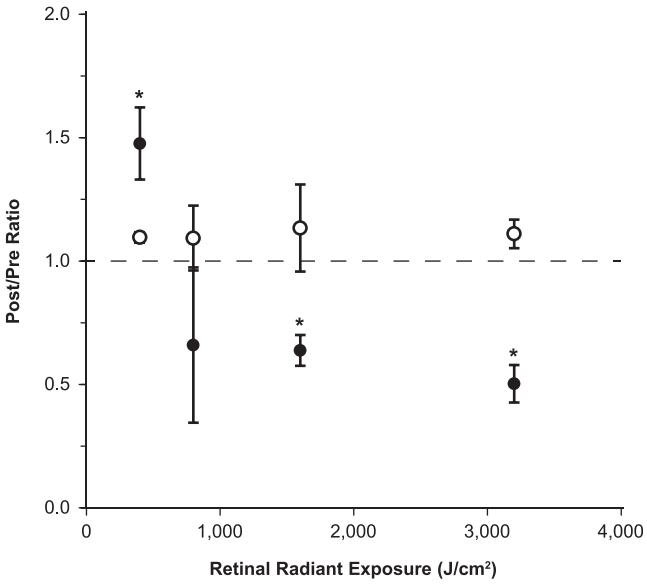

Figure 5. The ratio of the apparent density (*filled circles*) and initial recovery rate (*open circles*) measured after a 568-nm RRE to that measured before, plotted as a function of RRE. *Error bars* are SEM. *Asterisks* denote statistical significance when compared with unity.

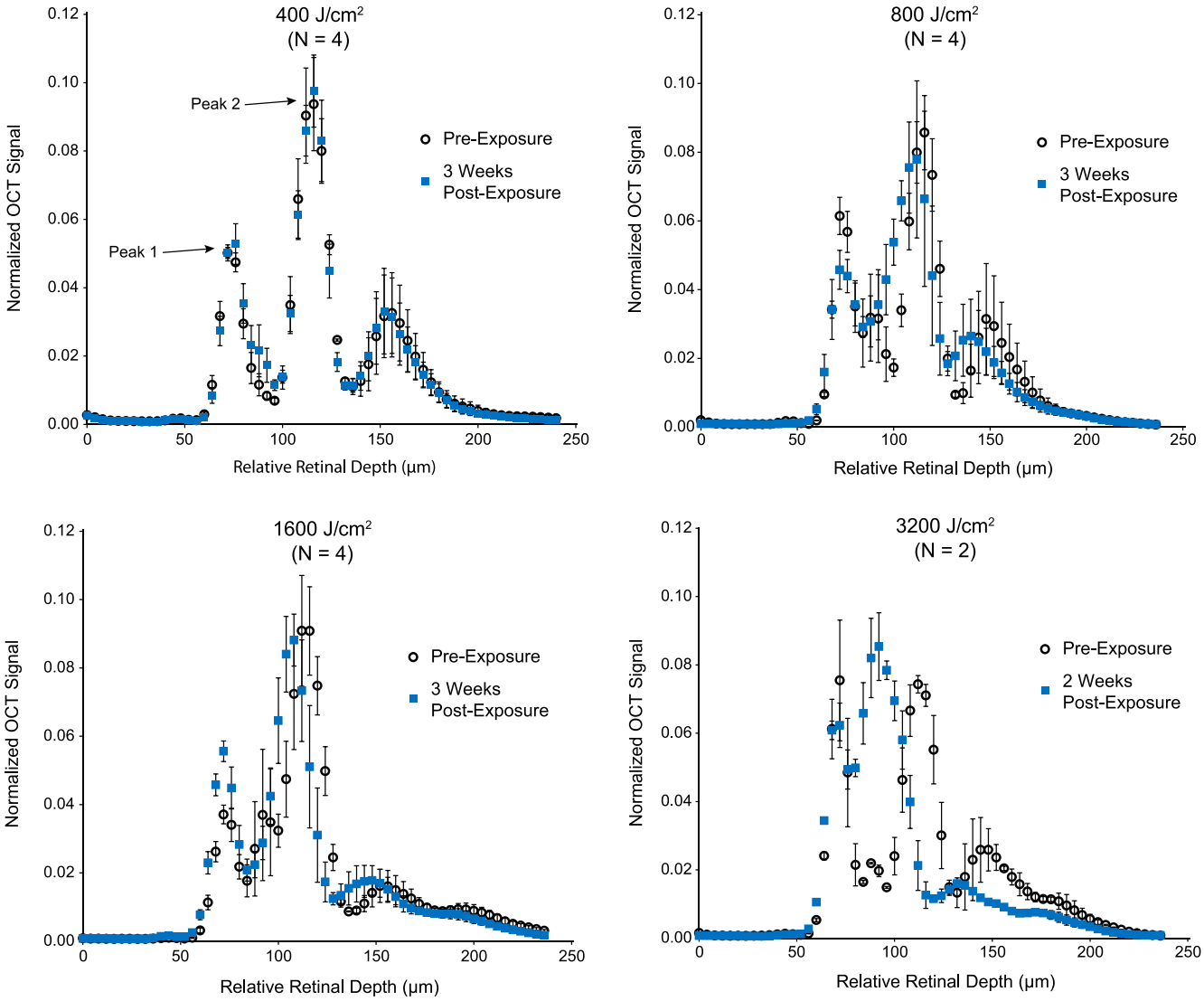

Figure 6. Plots showing OCT signal as a function of depth through the photoreceptors, RPE, and choroid. Pre-exposure (*open black circles*) and post exposure (*solid blue squares*) traces were aligned to peak 1. Retinal depth is reported relative to an arbitrary point in the outer nuclear layer. The distance between peaks 1 and 2 was significantly reduced after 568-nm exposures of 800, 1600, and 3200 J/cm^2.

t-test, $P = 0.86$). However, these exposures did have a significant effect on the apparent density of rhodopsin in the tested regions (ANOVA, $P = 0.009$). To test for a significant change in density at each RRE, the ratio of the post exposure value to the pre-exposure value was calculated and compared with 1. Figure 5 shows the mean pre/post apparent density (filled circles) and initial recovery rate (open circles) ratios as a function of RRE. Exposures at 400 J/cm^2 showed a significant increase in apparent density of rhodopsin ($P = 0.047$). Exposures at 800 J/cm^2 showed no significant change in apparent density ($P = 0.36$). Exposures at 1600 and 3200 J/cm^2 showed significant decreases in apparent density ($P = 0.010$ and 0.007, respectively).

Figure 6 shows the mean outer retinal OCT signal as a function of depth generated from volumes recorded before and after each RRE. The signal intensity was normalized to the total power of the curve and the pre- and post-exposure curves were aligned by their first peaks. Retinal depth is reported in micrometers relative to an arbitrary position in the outer nuclear layer.

The relative separation of the two primary photoreceptor and RPE associated OCT peaks was measured at each retinal location, pre- and post-exposure. The mean pre-exposure distance between these peaks was 40.7 ± 0.5 μm. The mean distances measured after each exposure, in order of ascending RRE, were 39.9 ± 0.6, 31.4 ± 3.3, 34.0 ± 1.6, and 20.6 ± 2.7 μm. An ANOVA on these data showed a significant effect of RRE on optical path ($P < 0.001$). Compared with the pre-exposure condition, no significant change in the distance between these peaks was measured for exposures at 400 J/cm^2 ($P = 0.43$). Exposures at 800, 1600, and 3200 J/cm^2 all resulted in a significant decrease in relative peak distance ($P < 0.001$ for all three). These results are shown in Figure 7. No correlation was found between change in apparent density and change in optical path as measured by OCT ($P = 0.499$).

Discussion

Retinal pigment epithelium disruption occurs at RREs much lower than those that cause a measurable decrease in

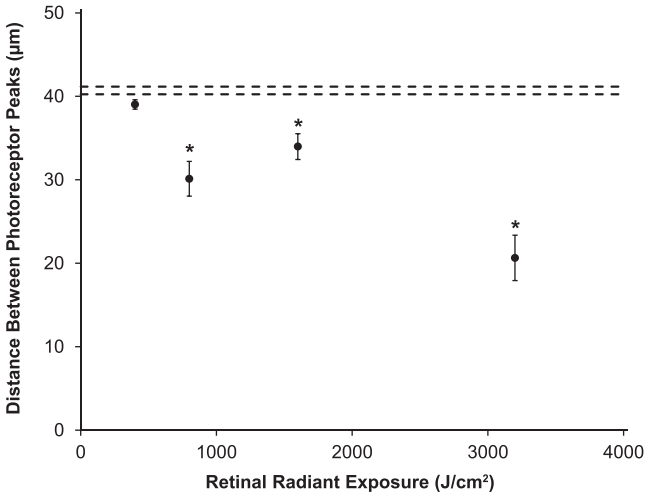

FIGURE 7. Plot showing the mean distance between OCT peaks 1 and 2 measured after each retinal radiant exposure. *Error bars* represent the standard error of the mean. The *dashed lines* define the standard error about the mean of all the pre-exposure measurements.

rhodopsin density. As can be seen in Figure 3, disruption occurred at all RREs tested in this study. As of Z136.1-2007, the ANSI photochemical MPE for a 568-nm exposure was 560 J/cm^2.[17] Thus, the highest RRE tested was 5.7 times the MPE and the lowest RRE was 70% of the photochemical MPE.[17,18] The ANSI standard has recently been updated to protect against these exposure levels.[19]

While RPE disruption was seen at all RREs, statistically significant decreases in apparent density were only measured at 1600 and 3200 J/cm^2. Mean apparent density increased significantly after the 400 J/cm^2 exposures, though this increase was only marginally significant ($P = 0.047$). This was surprising as we know of no precedent for light exposure causing an increase in the density of photopigment, but we cannot rule out this possibility. It is also possible, for example, that the true pigment density was constant but the amount of stray light that dilutes the apparent pigment density was somehow reduced by the light exposure.[11] Such a change in the relative reflectivity could also account for the less uniform appearance of the photoreceptor mosaic visible in the IR reflectance images taken after each RRE.

While the mean apparent density measured after the 800 J/cm^2 exposures was reduced as compared to the pre-exposure measurements, this was not a statistically significant effect. The variability of the 800 J/cm^2 measurements was much higher than that of the other three groups. Thus, the threshold RRE for a measurable density decrease lies somewhere between 400 and 1600 J/cm^2.

Despite these changes in absolute density and the appearance of RPE disruption, no measurable change in initial rhodopsin recovery rate was measured for any of the retinal radiant exposures tested. These results suggest that the appearance of RPE disruption does not necessarily signify an associated loss in photoreceptor and RPE function. Photopigment regeneration in rods relies heavily on the RPE for delivery of 11-*cis* retinal. Yet, 2 weeks after an apparent photochemical effect on the RPE, the rods are able to recover from a bleach at the same rate as before the insult. The RPE likely either remains functional after these exposures (at least in terms of their role in the retinoid cycle) or has recovered function within 2 weeks. Even at exposure levels that caused a measureable change in density, the retinoid cycle appears to still be active. These results suggest that some visual function is likely to have been preserved within the affected retinal regions, though this has not been confirmed psychophysically.

The OCT measurements made in conjunction with this densitometry study provide additional evidence for structural changes associated with RPE disruption. The correspondence between signal peaks in OCT volume data from the outer retina and real anatomical structures of the photoreceptors and RPE is currently a matter of debate. At the peripheral eccentricities tested in this study, as many as three scattering layers have been measured between the external limiting membrane (ELM) and the choroid. There is general agreement that the third peak after the ELM (labeled peak 2 in Fig. 1) represents the point where the outer segment tips insert into the RPE.[20–22] The two peaks vitread to the RPE are thought to be associated with the photoreceptors. The most commonly used interpretation suggests that the first peak after the ELM (labeled peak 1 in Fig. 1) defines the interface between the inner and outer segments of the photoreceptors. The next peak (intermediate between peaks 1 and 2 and not visible in Fig. 1) was only occasionally visible and was not used in our analysis. Human histologic measurements by Curcio et al.[23] show that the length of the rod outer segments at these eccentricities is approximately 30 μm, somewhat shorter than the 40 μm we measured. This suggests that the slice of retina we have measured incorporates the outer segments as well as part of the RPE and/or inner segments.

The change in distance between the primary OCT photoreceptor peaks suggests a reduction in the optical thickness of this layer at higher RREs. This reduction could result from several underlying mechanisms including a reduction in the refractive index of that layer. Another possibility is that the refractive index is unchanged but the actual thickness of the layer is reduced, such as would occur if the outer segments were shortened or if they were bent. There is histologic evidence in support of this latter hypothesis. Hunter et al.[1] showed that 568-nm radiant exposures at 788 J/cm^2 could produce a thickening of the RPE layer, causing the outer segments to become disorganized and tilted (Fig. 8).

The small sample size and the large inherent variability of the densitometry data make a detailed quantitative comparison with the OCT results difficult. However, the OCT data suggest a thinning of the outer retina under the same high light exposures that produce a reduction in apparent pigment density with retinal densitometry. For example, if the RPE had in fact disrupted rod orientation, the ability of the rod to waveguide light along the entire length of the outer segment may have been compromised, reducing apparent density. It is also possible that the outer segments are simply shorter or that the concentration of rhodopsin within the rods is affected by RRE. We cannot rule out other possibilities, such as changes in reflectance of layers within the outer retina in front of and behind the photopigment.

Despite the changes in apparent density with RRE, the fact that we observed no changes in the rate of regeneration of rod pigment suggests that the visual cycle is intact. The RPE seems to be capable of servicing the rods in the exposed area. It should be noted, however, that we are averaging reflectance measured over tens of cells and that this prevents us from discriminating variations that may be occurring within the exposed region. For example, it may be that the preserved rhodopsin regeneration is occurring only at the edge of the exposed region. This would suggest that those photoreceptors were receiving retinoid from RPE cells that were less effected or unaffected by the disrupting exposure, while those in the center of the region may not be receiving retinoid at all. Such a possibility cannot be ruled out with our current data.

Investigative Ophthalmology & Visual Science

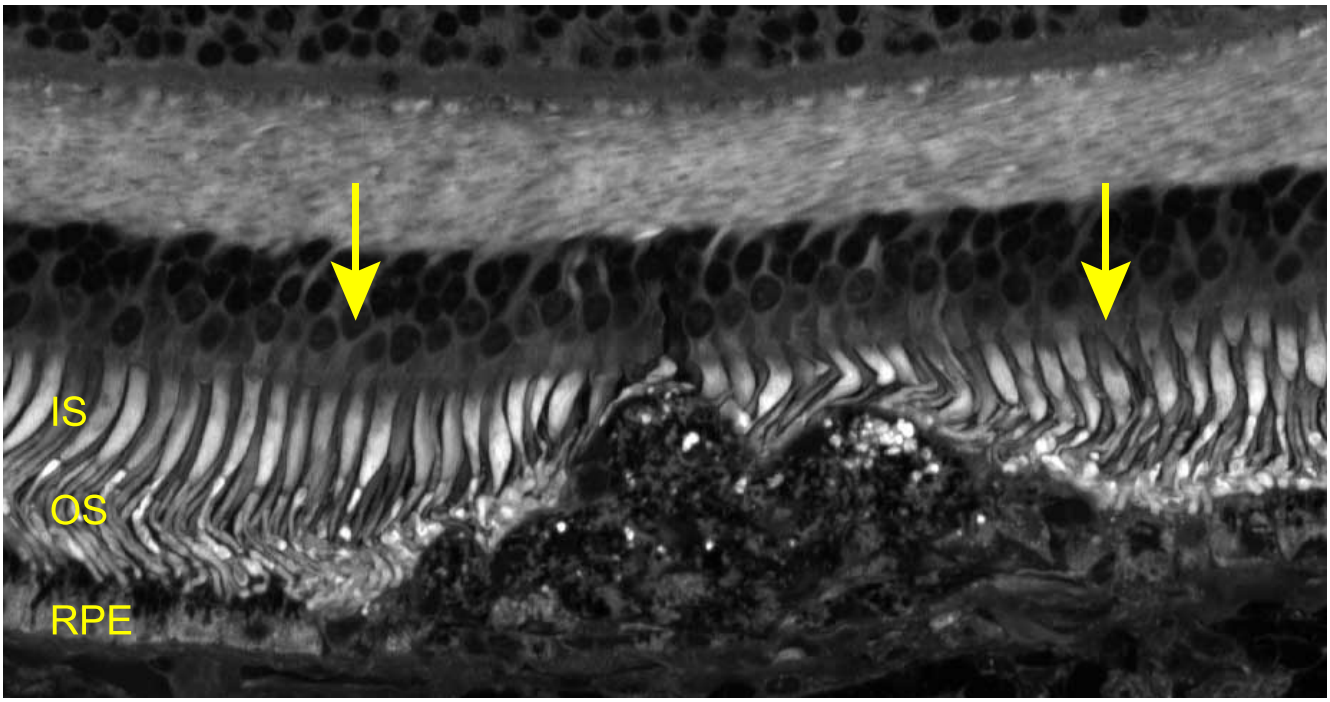

FIGURE 8. Differential interference contrast image of a histologic section of monkey retina recorded after RRE of 788 J/cm^2 at 568 nm. In this example, the RPE is no longer visible and a mass of material has expanded toward the inner retina, displacing the photoreceptors. The two *arrows* denote the edges of the exposed region. The labels represent the inner segments (IS) and outer segments (OS) of the photoreceptors and the RPE.

CONCLUSIONS

We found that light exposures near threshold, but intense enough to disrupt RPE autofluorescence do not necessarily impact function of the outer retina, at least as assessed with AO retinal densitometry. At higher light exposures, changes in apparent density are obvious, though these do not seem to be associated with changes in the kinetics of the visual cycle. Nonetheless, it is advisable to avoid visible light exposures that may cause RPE disruption, as is recommended in the latest version of the ANSI standard.[19]

Acknowledgments

The authors thank Lee Anne Schery, Jessica Morgan, and William S. Fischer for their assistance. This work was supported by the National Institute of Health (Bethesda, MD, USA) through the Grants BRP-EY014375, R01-EY022371, R01-EY004367, K23-EY016700, P30-EY001319, and T32-EY07125. The image registration software used to produce our AOSLO images, DeMotion, was developed by Alfredo Dubra and Zach Harvey with funding from Research to Prevent Blindness (New York, NY, USA) and the National Institute of Health through the Grants BRP-EY014375 and 5 K23 EY016700. Alfredo Dubra and Kamran Ahmad developed the adaptive optics control software.

Disclosure: **B.D. Masella**, Canon, Inc. (F); **J.J. Hunter**, Polgenix, Inc. (F), Canon, Inc. (F), P; **D.R. Williams**, Polgenix, Inc. (F), Canon, Inc. (F), Pfizer (C, R), P

References

1. Hunter JJ, Morgan JI, Merigan WH, Sliney DH, Sparrow JR, Williams DR. The susceptibility of the retina to photochemical damage from visible light. *Progr Retin Eye Res*. 2012;31:28–42.
2. Rushton WA. A cone pigment in the protanope. *J Physiol*. 1963;168:345–349.
3. Rushton WA. The density of chlorolabe in the foveal cones of the protanope. *J Physiol*. 1963;168:360–373.
4. Alpern M. Rhodopsin kinetics in the human eye. *J Physiol*. 1971;217:447–471.
5. van Norren D, van de Kraats J. A continuously recording retinal densitometer. *Vision Res*. 1981;21:897–905.
6. van Norren D. Towards improved instrumentation for retinal densitometry. *Adv Biosci*. 1987;62:177–179.
7. Mahroo OA, Lamb TD. Recovery of the human photopic electroretinogram after bleaching exposures: estimation of pigment regeneration kinetics. *J Physiol*. 2004;554:417–437.
8. Lamb TD, Pugh EN Jr. Dark adaptation and the retinoid cycle of vision. *Progr Retin Eye Res*. 2004;23:307–380.
9. Lamb TD, Pugh EN Jr. Phototransduction, dark adaptation, and rhodopsin regeneration the proctor lecture. *Invest Ophthalmol Vis Sci*. 2006;47:5137–5152.
10. Morgan JI, Pugh EN Jr. Scanning laser ophthalmoscope measurement of local fundus reflectance and autofluorescence changes arising from rhodopsin bleaching and regeneration. *Invest Ophthalmol Vis Sci*. 2013;54:2048–2059.
11. Masella BD, Hunter JJ, Williams DR. New wrinkles in retinal densitometry. *Invest Ophthalmol Vis Sci*. 2014;55:7525–7534.
12. Morgan JI, Hunter JJ, Masella B, et al. Light-induced retinal changes observed with high-resolution autofluorescence imaging of the retinal pigment epithelium. *Invest Ophthalmol Vis Sci*. 2008;49:3715–3729.
13. Hunter JJ, Masella B, Dubra A, et al. Images of photoreceptors in living primate eyes using adaptive optics two-photon ophthalmoscopy. *Biomed Opt Express*. 2010;2:139–148.
14. Morgan JI, Dubra A, Wolfe R, Merigan WH, Williams DR. In vivo autofluorescence imaging of the human and macaque retinal pigment epithelial cell mosaic. *Invest Ophthalmol Vis Sci*. 2009;50:1350–1359.
15. Michaelis L, Menten ML. Die Kinetik der Invertinwirkung. *Biochemische Zeitschrift*. 1913;49:333–369.

16. Morgan JI, Hunter JJ, Merigan WH, Williams DR. The reduction of retinal autofluorescence caused by light exposure. *Invest Ophthalmol Vis Sci*. 2009;50:6015–6022.
17. American National Standard Institute. American National Standard for Safe Use of Lasers ANSI Z136.1-2007. Orlando, FL: Laser Institute of America; 2007.
18. Ham WT, Mueller HA, Ruffolo JJ, Clarke AM. Sensitivity of the Retina to Radiation-Damage as a Function of Wavelength. *Photochem Photobiol*. 1979;29:735–743.
19. American National Standard Institute. American National Standard for Safe Use of Lasers ANSI Z136.1-2014. Orlando, FL: Laser Institute of America; 2014.
20. Drexler W, Sattmann H, Hermann B, et al. Enhanced visualization of macular pathology with the use of ultrahigh-resolution optical coherence tomography. *Arch Ophthalmol*. 2003;121:695–706.
21. Ko TH, Fujimoto JG, Duker JS, et al. Comparison of ultrahigh- and standard-resolution optical coherence tomography for imaging macular hole pathology and repair. *Ophthalmology*. 2004;111:2033–2043.
22. Jonnal RS, Kocaoglu OP, Wang Q, Lee S, Miller DT. Phase-sensitive imaging of the outer retina using optical coherence tomography and adaptive optics. *Biomed Opt Express*. 2012;3:104–124.
23. Curcio CA, Sloan KR, Kalina RE, Hendrickson AE. Human photoreceptor topography. *J Comp Neurol*. 1990;292:497–523.

Investigative Ophthalmology & Visual Science